Ablation of insulin receptor substrates 1 and 2 suppresses *Kras*-driven lung tumorigenesis

He Xu[a,b,1], Min-Sik Lee[a,b,1], Pei-Yun Tsai[a,b], Ashley S. Adler[a], Natasha L. Curry[a], Saketh Challa[a], Elizaveta Freinkman[c,2], Daniel S. Hitchcock[d], Kyle D. Copps[a,b], Morris F. White[a,b], Roderick T. Bronson[e], Michael Marcotrigiano[f], Yaotang Wu[f], Clary B. Clish[d], and Nada Y. Kalaany[a,b,d,3]

[a]Center for Basic and Translational Obesity Research, Division of Endocrinology, Boston Children's Hospital, Boston, MA 02115; [b]Department of Pediatrics, Harvard Medical School, Boston, MA 02115; [c]Whitehead Institute for Biomedical Research, Cambridge, MA 02142; [d]Broad Institute of MIT and Harvard, Cambridge, MA 02142; [e]Department of Pathology, Tufts University Schools of Medicine and Veterinary Medicine, North Grafton, MA 01536; and [f]Department of Radiology, Boston Children's Hospital and Harvard Medical School, Boston, MA 02115

Edited by Anton Berns, The Netherlands Cancer Institute, Amsterdam, The Netherlands, and approved March 9, 2018 (received for review October 20, 2017)

Non–small-cell lung cancer (NSCLC) is a leading cause of cancer death worldwide, with 25% of cases harboring oncogenic Kirsten rat sarcoma (*KRAS*). Although KRAS direct binding to and activation of PI3K is required for *KRAS*-driven lung tumorigenesis, the contribution of insulin receptor (IR) and insulin-like growth factor 1 receptor (IGF1R) in the context of mutant *KRAS* remains controversial. Here, we provide genetic evidence that lung-specific dual ablation of insulin receptor substrates 1/2 (*Irs1*/*Irs2*), which mediate insulin and IGF1 signaling, strongly suppresses tumor initiation and dramatically extends the survival of a mouse model of lung cancer with *Kras* activation and *p53* loss. Mice with *Irs1*/*Irs2* loss eventually succumb to tumor burden, with tumor cells displaying suppressed Akt activation and strikingly diminished intracellular levels of essential amino acids. Acute loss of *IRS1*/*IRS2* or inhibition of IR/IGF1R in *KRAS*-mutant human NSCLC cells decreases the uptake and lowers the intracellular levels of amino acids, while enhancing basal autophagy and sensitivity to autophagy and proteasome inhibitors. These findings demonstrate that insulin/IGF1 signaling is required for *KRAS*-mutant lung cancer initiation, and identify decreased amino acid levels as a metabolic vulnerability in tumor cells with IR/IGF1R inhibition. Consequently, combinatorial targeting of IR/IGF1R with autophagy or proteasome inhibitors may represent an effective therapeutic strategy in *KRAS*-mutant NSCLC.

non–small-cell lung cancer | *Kras* | insulin receptor substrates | autophagy | amino acids

Non–small-cell lung cancer (NSCLC) accounts for the majority of lung cancer, which to date remains the leading cause of cancer death in the United States and worldwide (1, 2). About a quarter of NSCLC cases harbor Kirsten rat sarcoma (*KRAS*) activating mutations (3, 4). However, effective therapies targeting KRAS are still lacking and alternative approaches are urgently needed (5). Previous reports showed that KRAS can directly bind to and activate the p110α catalytic subunit of PI3K and that this interaction is required for in vivo *Kras*-driven tumor initiation and maintenance in mouse models of lung cancer (6, 7). However, the sufficiency of KRAS–PI3K interaction in driving lung cancer development remains largely controversial, with evidence from cell culture studies implicating additional input from insulin receptor (IR) and insulin-like growth factor 1 receptor (IGF1R) (8, 9). Most insulin/IGF1 signaling in the lungs converges intracellularly onto the adaptor proteins insulin receptor substrates IRS1 and IRS2 (10) before diverging to a complex network of downstream signaling effectors, including PI3K/AKT (11). Here, using a robust genetic approach, we provide evidence that concomitant ablation of *Irs1* and *Irs2* in the lungs of a well-established genetically engineered mouse model of lung cancer with conditional *Kras* activation and *p53* loss strongly suppresses tumor initiation, doubling tumor latency and significantly extending survival. Lung cells with *Irs1*/*Irs2* ablation eventually overcome this suppression, although at a stochastic rate, forming advanced lung adenocarcinomas. Interestingly, cells derived from these tumors not only display suppressed Akt activation in response to insulin/IGF1 stimulation but also significantly decreased intracellular levels of essential amino acids. We find that acute loss or knockdown of *IRS1*/*IRS2* in *KRAS*-mutant human NSCLC cells, or pharmacological inhibition of IR/IGF1R in *KRAS*-mutant NSCLC or murine lung cancer cells results in the decreased uptake and intracellular levels of essential amino acids, accompanied by enhanced basal autophagy. NSCLC cells with acute loss of *IRS1*/*IRS2* also display increased sensitivity to lysosomal and proteasomal inhibitors. Our findings provide evidence that *IRS1* and *IRS2* are required for *KRAS*-mutant lung cancer formation. They further shed light on the metabolic vulnerabilities that arise in tumors treated with IR/IGF1R inhibitors, pointing to potential combinatorial approaches for treating *KRAS*-driven NSCLC.

Significance

To date, therapies are lacking that efficiently target the Kirsten rat sarcoma (*KRAS*) oncogene, which is responsible for approximately a quarter of all lung cancer cases in the United States. This study provides genetic evidence that the insulin/insulin-like growth factor 1 (IGF1) signaling, which modulates cellular survival, growth, and metabolism, is required for *KRAS*-driven lung cancer initiation. It further identifies a metabolic vulnerability in tumors with loss of such signaling, that is, the dependence on autophagy (a self-eating process), and protein degradation, to compensate for decreased amino acid levels. Such vulnerability could be exploited therapeutically using available autophagy and protein degradation inhibitors, in combination with insulin receptor/IGF1 receptor inhibitors, in patients with *KRAS*-mutant lung cancer.

Author contributions: N.Y.K. conceived and supervised the study; N.Y.K. designed research; H.X., M.-S.L., P.-Y.T., A.S.A., and N.L.C. performed research; P.-Y.T. and A.S.A. assisted with in vivo experiments; S.C. quantified tumor burden imaged by MRI; M.M. and Y.W. assisted with mouse lung MRI; E.F. and D.S.H. performed metabolite quantification analyses; C.B.C. supervised metabolite quantification analyses; K.D.C. assisted with the Luminex assay; K.D.C., M.F.W., M.M., and Y.W. contributed new reagents/analytic tools; N.L.C. generated the mice and performed preliminary work; M.F.W. provided floxed *Irs1/2* mice; H.X., M.-S.L., P.-Y.T., A.S.A., N.L.C., S.C., E.F., D.S.H., R.T.B., C.B.C., and N.Y.K. analyzed data; and H.X. and N.Y.K. wrote the paper.

The authors declare no conflict of interest.

This article is a PNAS Direct Submission.

[1]H.X. and M.-S.L. contributed equally to this work.

[2]Present address: Metabolon, Inc., Research Triangle Park, NC 27709.

[3]To whom correspondence should be addressed. Email: nada.kalaany@childrens.harvard.edu.

This article contains supporting information online at www.pnas.org/lookup/suppl/doi:10.1073/pnas.1718414115/-/DCSupplemental.

Published online April 2, 2018.

Results

Lung-Specific Genetic Ablation of *Irs1* and *Irs2* Significantly Delays Tumor Formation in a *Kras*-Driven Mouse Model of Lung Cancer. The conditional genetically engineered mouse model of lung cancer *Lox-STOP-Lox* (*LSL*)-$Kras^{G12D/+}$;$p53^{fl/fl}$ (12–14), herein referred to as "KP," was bred to mice harboring floxed alleles for both *Irs1* and *Irs2* genes (15), leading to the generation of $Kras^{G12D/+}$;$p53^{fl/fl}$;$Irs1^{fl/fl}$;$Irs2^{fl/fl}$ or "KPI" mice. Intranasal administration of adenoviral Cre into KP or KPI mice at 5–6 wk of age led to the concomitant expression of activated *Kras* and loss of *p53* alone (KP mice) or the triple loss of *p53*, *Irs1*, and *Irs2* (KPI mice) in mouse lung cells (Fig. 1*A*). As previously reported (14, 16), 10 wk post-Cre administration, KP mice developed extensive lung adenomas and adenocarcinomas (Fig. 1 *B* and *C*) and succumbed to tumor burden by 140 d, with median survival of 107 or 103 d for males and females, respectively (Fig. 1*D*). In contrast, lungs of KPI mice were devoid of any tumors or hyperplasia at 8–10 wk postinfection and retained normal histology (Fig. 1 *B*, *C*, *E*, and *F*). Surprisingly, however, KPI mice eventually overcame the loss of *Irs1*/*Irs2* and developed lung adenocarcinomas at a significantly extended and highly variable tumor latency (16–30 wk for KPI compared with 8 wk for KP; Fig. 1 *E* and *F*). Moreover, both the median survival (191 d for males and 209 d for females) and maximal survival (~300 d) of KPI mice were twice as long as those of KP mice (Fig. 1*D*). Interestingly, when lung tumors from moribund KP and KPI mice were analyzed and compared histopathologically, KPI tumors displayed a significantly increased proportion of higher-grade adenocarcinomas and carcinomas, characterized by nuclear pleomorphism and invasion of basement membrane (Fig. 1 *G* and *H*). These results indicate that *Irs1* and *Irs2* are required for *Kras*-driven lung tumor initiation and that *Kras*-transformed cells can eventually bypass *Irs1*/*Irs2* loss, developing more aggressive tumors at a highly variable and extended latency.

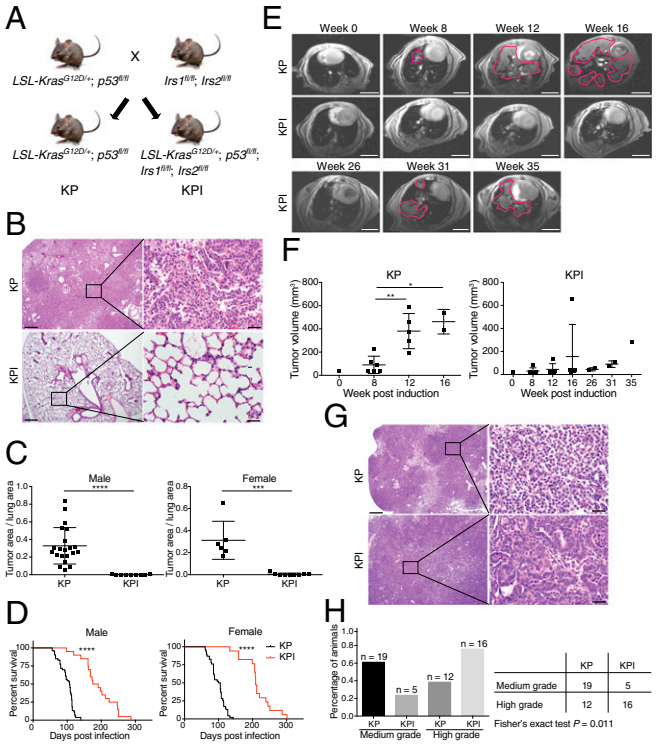

Fig. 1. Loss of *Irs1* and *Irs2* significantly delays *Kras*-driven lung tumorigenesis. (*A*) Breeding schematic for KP and KPI mice. (*B*) H&E staining of KP and KPI lungs 10 wk postadenoviral Cre infection (*Left*) with 10-fold magnification of framed area (*Right*). [Scale bars: 400 μm (*Left*) and 40 μm (*Right*).] (*C*) Tumor burden in KP and KPI lungs 10 wk postadenoviral Cre infection. Males, $n = 21$ (KP) and $n = 9$ (KPI); females, $n = 6$ (KP) and $n = 9$ (KPI); $^{***}P < 0.001$; $^{****}P < 0.0001$. (*D*) Kaplan–Meier survival curves. Males, $n = 53$ (KP) and $n = 20$ (KPI); females, $n = 46$ (KP) and $n = 17$ (KPI); $^{****}P < 0.0001$ by log-rank test. (*E*) MRI showing axial planes of representative KP lungs at weeks 0–16, and KPI lungs at weeks 0–35 postadenoviral Cre infection. Tumor areas are delineated in red. (Scale bars: 5 mm.) (*F*) Volumes of KP and KPI tumors quantified from MRI images represented in *E*. Each data point represents one animal. $^{*}P < 0.05$; $^{**}P < 0.01$. (*G*) H&E staining of KP and KPI lungs from moribund mice (*Left*) with 10-fold magnification of framed area (*Right*). [Scale bars: 400 μm (*Left*) and 40 μm (*Right*).] (*H*) Percentage of KP and KPI mice with medium- or high-grade tumors at moribund stage (*Left*) with Fisher's exact test (*Right*). In *C* and *F*, data represent the mean ± SD. H&E, hematoxylin and eosin.

Loss of *Irs1* and *Irs2* Suppresses Akt Signaling and Leads to Decreased Amino Acid Levels in Murine *Kras*-Driven Lung Tumor Cells. To characterize the signaling and metabolism of cells with *Irs1*/*Irs2* loss, KP and KPI lung tumors were isolated and used to establish several cell lines in culture. Genotyping confirmed the concomitant excision of the STOP codon upstream of $Kras^{G12D}$ and loss of *p53* in both KP and KPI cells, with the additional deletion of *Irs1* and *Irs2* in KPI but not KP cells, thus validating that the KPI tumors did not escape *Irs1*/*Irs2* loss (Fig. S1*A*). Although one of the KPI cell lines (KPI-6) seemed to harbor incomplete Cre-mediated recombination, the faint genotyping bands for LSL-$Kras^{G12D}$ and floxed *Irs1* and *Irs2* were due to the rare residual presence of nontransformed cells at this early cell line passage. Indeed, in future passages, Irs1 and Irs2 proteins were completely lost in all KPI cell lines tested (Fig. 2*A* and Fig. S1*B*).

To confirm the relevance and engagement of Irs1 and Irs2 in insulin/IGF1 signaling in lung tumor cells, we first performed a Luminex bead-based immunoassay (17) in KP and KPI cell lines that is optimized to assess the interaction between Irs1 and Pi3k catalytic subunit p110α (Fig. S1*C*). Acute stimulation of serum-starved KP but not KPI cells with either insulin or IGF1 dramatically enhanced Irs1-p110α interaction, confirming signal transduction from Igf1r to Pi3k in the lung cancer cells (Fig. S1*C*). We then assessed alterations in Akt phosphorylation (pT308 and pS473) upon ligand stimulation in KP and KPI cells with single or double knockdown of *Irs1* and *Irs2*. Loss of either *Irs1* or *Irs2* alone did not significantly affect Akt activation in the murine KP cells (Fig. S2) or in human *KRAS*-mutant NSCLC cells (Fig. S3). In contrast, concomitant silencing of both *Irs1* and *Irs2* strongly suppressed Akt activation in response to insulin or IGF1 stimulation (Fig. 2*A*). These results provide evidence of a functional redundancy in Irs1 and Irs2 signal transduction in *Kras*-driven lung tumor cells, and are consistent with a recent report demonstrating increased rather than decreased tumor formation in a *Kras*-driven mouse model of lung cancer with loss of *Irs1* alone (18). Intriguingly, however, Erk1/2 activation (pT202/Y204) levels varied significantly among the different cell lines upon ligand treatment, and did not correlate with the loss of *Irs1*/*Irs2*, reflecting heterogeneity in the tumor cell populations (Fig. 2*A* and Figs. S2 and S3). This observation is consistent with the previously reported intratumoral stage-heterogeneity in *Kras*-driven lung tumors, where MAPK signal amplification, a driver of malignant progression, was found to only mark a fraction of the tumor cell populations (19).

To acquire a broader assessment of the effects of *Irs1* and *Irs2* loss on signaling networks, we performed reverse-phase protein array (RPPA) analysis (20) of 300 proteins and phosphoproteins representing many major signaling pathways (Fig. 2*B* and Dataset S1). We used protein lysates from KP and KPI cells that were either nonstarved (10% serum), 1-h serum-starved or serum-starved and acutely stimulated with IGF1. The most striking differences were detected under acute IGF1-stimulated conditions, representing significant suppression of Akt activation and its downstream signaling in KPI compared with KP cells. As expected, IGF1 stimulation resulted in the phosphorylation of its receptor at Y1135/1136 in both KP and KPI cells (Fig. 2*B*). However, Akt activation (pT308 and S473) upon IGF1 stimulation was blunted in KPI, compared with KP cells. This was mirrored by the blunted

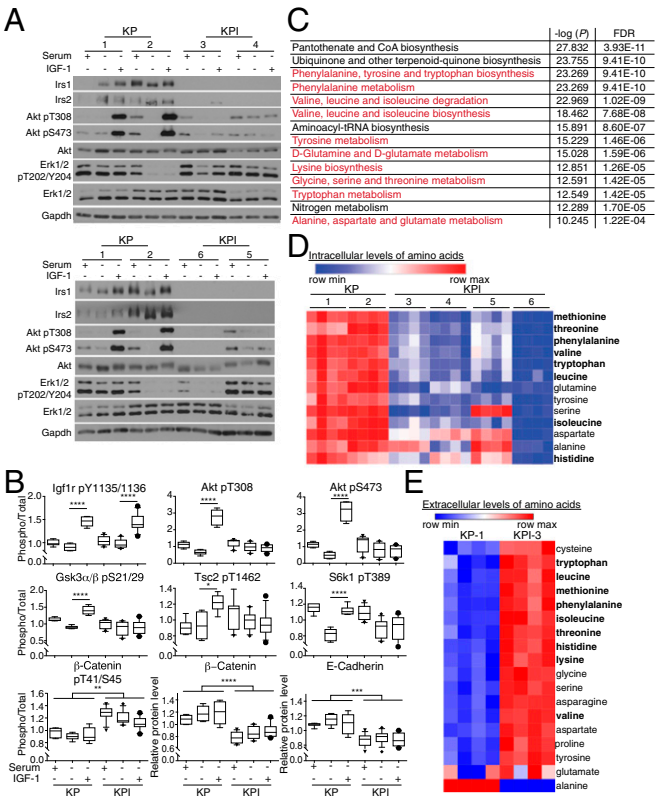

Fig. 2. Murine *Irs1*/*Irs2*-null *Kras*-driven lung tumor cells have impaired Akt signaling and decreased intracellular amino acid levels. (*A*) Levels of Irs1, Irs2, total or phosphorylated Akt and Erk1/2 in KP and KPI cells grown in 10% serum or serum-starved for 1 h with or without IGF1 (50 ng/mL) stimulation for 10 min. Gapdh was used as a loading control. (*B*) Box plots representing total or phosphorylated levels of selected effectors of Akt signaling quantified by reverse-phase protein array (RPPA) in KP and KPI cells treated as in *A*. Levels of phosphorylated proteins were normalized to total levels of the respective proteins. Data represent the median ±10th to 90th percentile for each protein/phosphoprotein; $n = 3$ biological replicates per condition per cell line. *$P < 0.05$; **$P < 0.01$; ***$P < 0.001$; ****$P < 0.0001$. (*C*) List of top 14 metabolic pathways that are significantly different between KP (-1, -2) and KPI (-3 to -6) cells grown in 10% serum for 24 h. In red are pathways involved in amino acid metabolism. Data were processed by Metaboanalyst 3.0, and pathways were ranked by −log of the *P* value. FDR indicates false-discovery rate. (*D* and *E*) Heat maps listing in descending order of statistical significance ($P < 0.05$ by *t* test) amino acids whose intracellular (*A*) or extracellular media (*B*) levels are different between KP and KPI cells described in *C*. In bold are essential amino acids. Red indicates higher expression, and blue indicates lower expression relative to the mean expression level within each group; $n = 4$ biological replicates per cell line.

inactivating phosphorylation of the Akt targets, Gsk-3α/β (pS21/29) and Tsc2 (T1462). Indeed, the increased activity in KPI cells, of Tsc2, a repressor of mTORC1 signaling, led to decreased phosphorylation of the mTORC1 target S6k1 (T389) upon IGF1 stimulation, compared with KP cells (Fig. 2*B*). However, because mTORC1 can be activated by growth factor signaling independent of insulin/IGF1 (21), S6k1 phosphorylation was maintained in KPI cells cultured in 10% serum, independent of *Irs1*/*Irs2* loss. Consistent with suppressed Akt signaling in KPI cells, an increase in Gsk-3 α/β activity resulted in constitutive phosphorylation of β-catenin (T41/S45), which leads to its proteasomal degradation (Fig. 2*B*). Indeed, lower levels of β-catenin were detected in KPI cells, accompanied by a decrease in the levels of its binding partner E-cadherin (Fig. 2*B*). Interestingly, this phenotype is known to correlate with tumor progression (22) and a transition to a more mesenchymal, invasive phenotype (23), consistent with the more aggressive nature of KPI tumors at a moribund stage (Fig. 1 *G* and *H*).

We then sought to explore the metabolic differences between KP and KPI cells, with the goal of identifying metabolic dependencies upon *Irs1*/*Irs2* loss. To that end, we profiled over 150 polar metabolites in the tumor cells grown for 24 h under either non–serum-starved or serum-starved conditions. KP and KPI cells displayed no significant metabolic changes under serum-starved conditions, indicating that loss of *Irs1*/*Irs2* closely mimics conditions of growth factor deprivation. In contrast, striking differences were observed under nonstarved conditions, with pathway enrichment analysis identifying amino acid synthesis or degradation as top impacted metabolic pathways between KP and KPI cells (Fig. 2*C*). In particular, KPI cells exhibited significantly lower intracellular levels of essential amino acids, including leucine, isoleucine, valine, methionine, phenylalanine, threonine, tryptophan, in addition to glutamine and tyrosine (Fig. 2*D*), suggesting a role for Irs1/Irs2 in amino acid uptake and/or metabolism. Indeed, in contrast to their intracellular levels, extracellular media levels of most amino acids were strikingly higher in KPI compared with KP cells (Fig. 2*E*), implying a decrease in amino acid uptake upon *Irs1*/*Irs2* loss. These results are consistent with previous reports describing regulation of amino acid transport in diverse cell types by different growth factors, including insulin/IGF1 (24–27).

Loss of *IRS1* and *IRS2* in Human *KRAS*-Mutant NSCLC Cells Leads to Impaired AKT Signaling and Reduced Intracellular Amino Acid Levels. To investigate the relevance of IRS1 and IRS2 in human lung cancer, we extended our studies to established NSCLC cell lines that harbor activating *KRAS* mutations. Dual loss of *IRS1* and *IRS2* was engineered via CRISPR/Cas9 double knockout (DKO) in A549 cells (Fig. 3*A*), whereas *IRS1*/*IRS2* double knockdown (DKD) was achieved via stable small hairpin expression in both A549 and Calu-1 cells (Fig. 3*A* and Fig. S4 *A*–*C*). In A549 DKO, A549 DKD, and Calu-1 DKD cells, AKT activation was severely mitigated in response to insulin or IGF1 stimulation (Fig. 3*A* and Fig. S4 *A* and *B*), consistent with the results obtained from murine KP and KPI cells (Fig. 2*A*). Furthermore, in vitro cellular proliferation was impaired by loss of *IRS1*/*IRS2* (Fig. 3*B* and Fig. S4*D*).

To assess the effects of loss of *IRS1* and *IRS2* on cellular metabolism, metabolite profiling was performed on A549 and Calu-1 cells cultured under non–serum-starved conditions. Strikingly, and consistent with our findings in the mouse KPI cells, the intracellular levels of all essential amino acids, except for lysine, were significantly decreased or trended toward a decrease in A549 DKO and Calu-1 DKD cells compared with the control cells (Fig. 3*C*). This was accompanied by a moderate yet consistent decrease in the uptake of extracellular amino acids from the media (Fig. S5*A*). Furthermore, supplementation of their media with essential branched-chain amino acids (BCAAs) (i.e., leucine, isoleucine and valine) partially rescued the growth of A549 DKO and Calu-1 DKD cells (Fig. 3*D*). These results led us to investigate a potential regulation of amino acid transporter expression levels by loss of *IRS1*/*IRS2*. Although a variety of such transport systems exist that display overlapping substrate specificity, two of the mostly extensively studied are the SLC7A5 (LAT-1)/SLC3A2 heterodimer, which mediates the uptake of large neutral amino acids (including BCAAs), and SLC7A1 (CAT-1), a cationic amino acid (arginine, histidine, lysine) transporter. Loss of *IRS1*/*IRS2* in A549 DKO cells resulted in a significant decrease in the protein levels of SLC7A5 and SLC3A2, and a concomitant increase in SLC7A1 levels (Fig. S5*B*). However, despite similarly affecting amino acid uptake (Fig. 3*C* and Fig. S5*A*), or cellular proliferation (Fig. 3*B* and Fig. S4*D*), silencing of *IRS1*/*IRS2* in A549 DKD or Calu-1 DKD cells did not lead to similar or consistent changes, indicating a potential effect on other transporters and/or regulation at the activity level. This is consistent with previous reports indicating growth factor regulation of amino acid transport systems in variety of cell types, at both the expression and activity levels (24–27).

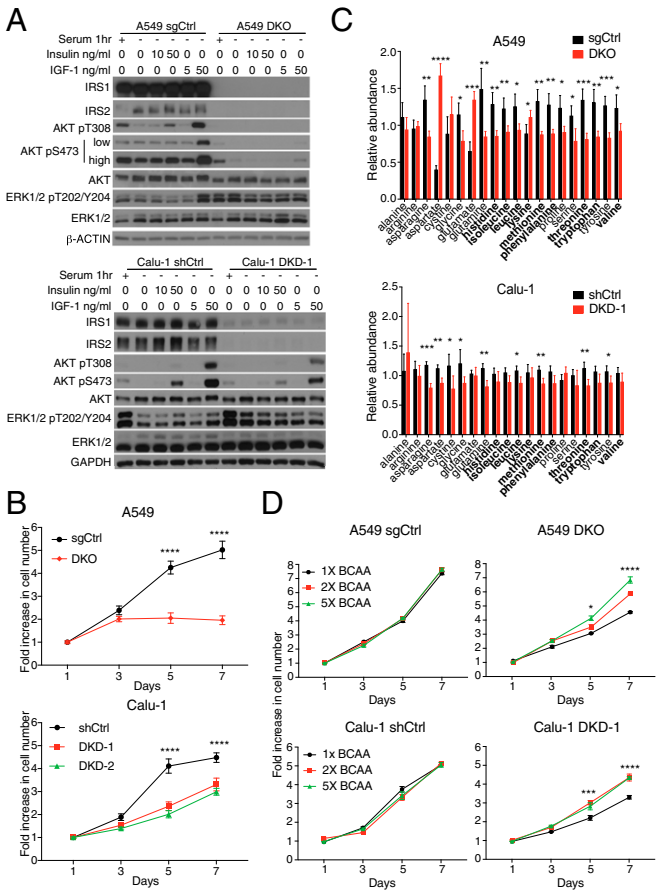

Fig. 3. Loss of *IRS1* and *IRS2* in human *KRAS*-mutant NSCLC leads to impaired AKT signaling and reduced intracellular amino acid levels. (*A*) Levels of IRS1, IRS2, total or phosphorylated AKT and ERK1/2 in NSCLC A549 cells with *IRS1*/*IRS2* (A549 DKO) or control (A549 sgCtrl) DKO as well as Calu-1 cells with *IRS1*/*IRS2* (Calu-1 DKD-1) or control (Calu-1 sh*GFP*/sh*Scramble*, termed shCtrl) DKD cells. Cells were serum-starved for 1 h and then stimulated with insulin or IGF1 for 10 min. β-ACTIN and GAPDH were used as loading controls. (*B*) Proliferation curves of cells described in *A* that were grown under low serum conditions (0.1% serum for A549 and 2% serum for Calu-1) over 7 d; $n = 6$. (*C*) Levels of amino acids in NSCLC cells described in *A* that were first normalized to protein levels, and then normalized to the median of all samples for each amino acid; $n = 4$ biological replicates per cell line; data are representative of two independent experiments. (*D*) Proliferation curves of cells described in *A* that were grown under low serum conditions (0.5% serum for A549 and 2% serum for Calu-1) in RPMI media containing either fivefold (5×), twofold (2×), or the standard (one-fold or 1×) concentrations of BCAAs: leucine (0.05 g/L), isoleucine (0.05 g/L), and valine (0.02 g/L) over 7 d; $n = 4$. In *B*–*D*, data represent the mean ± SD (*B* and *C*) or ±SEM (*D*). $^*P < 0.05$; $^{**}P < 0.01$; $^{***}P < 0.001$; $^{****}P < 0.0001$. In *B*, significance is between shCtrl and DKO or DKD conditions. In *D*, significance is between 1× BCAA and both 2× and 5× conditions.

Acute Loss of *IRS1* and *IRS2* Promotes Autophagy in Mouse and Human *KRAS*-Mutant Lung Cancer Cells. Because amino acid levels were significantly decreased upon *IRS1*/*IRS2* loss, we investigated a potential effect on autophagy, a self-catabolic process induced by nutrient starvation and decreased mTORC1 activity (28). We found that, compared with control cells, both A549 DKO and Calu-1 DKD cells are more sensitive to chloroquine (CQ) treatment, indicating that loss of *IRS1*/*IRS2* sensitizes NSCLC cells to autophagy inhibition (Fig. 4*A*). Indeed, A549 DKO cells demonstrated higher basal autophagic flux than control cells, as evidenced by increased levels and enhanced accumulation, in the presence of full media, of the autophagosome marker LC3-II upon CQ treatment (Fig. 4*B*). Moreover, upon GFP-LC3 overexpression, these cells demonstrated significantly higher levels of GFP cleavage independent of CQ treatment (Fig. 4*C*). Consistently, compared with control cells, a higher percentage of A549 DKO cells displayed GFP-LC3 punctae, resulting from enhanced autophagosome formation (Fig. 4 *D* and *E*). These results imply that NSCLC cells promote intracellular protein catabolic pathways to compensate for the sharp decrease in amino acid levels upon *IRS1*/*IRS2* loss. Indeed, compared with their respective control cells expressing *IRS1* and *IRS2*, both A549 DKO and Calu-1 DKD cells were more sensitive to the proteasome inhibitor MG-132 (Fig. 4*F*).

Inhibition of Insulin and IGF1 Signaling Hinders in Vivo NSCLC Growth and Sensitizes Tumors to Autophagy Inhibition. To assess whether acute inhibition of insulin/IGF1 signaling can result in a similar metabolic phenotype, murine KP cells (Fig. 5 *A* and *B*) and *KRAS*-mutant human NSCLC cells (Fig. 5 *C* and *D*) were treated with the pharmacological IR/IGF1R inhibitor NVP-AEW541. The latter led to enhanced basal autophagy detected by rapid accumulation of LC3B-II (Fig. 5 *A* and *C*). It also led to a significant decrease in intracellular amino acid levels (Fig. 5 *B* and *D*). These data indicate that acute suppression of insulin/IGF1 signaling decreases amino

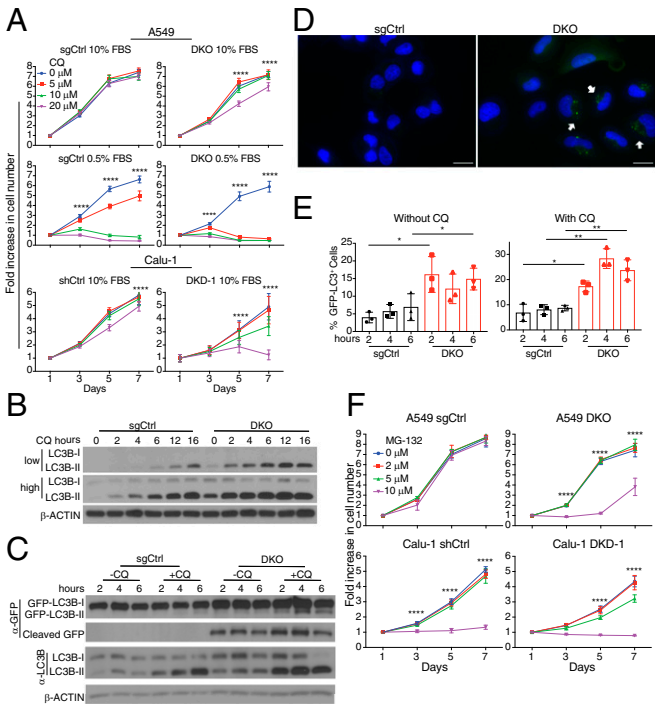

Fig. 4. Acute loss of *IRS1* and *IRS2* induces autophagy in human *KRAS*-mutant NSCLC cells. (*A*) Proliferation curves of NSCLC A549 DKO or sgCtrl cells as well as Calu-1 DKD or shCtrl cells cultured in 10% serum and treated with chloroquine (CQ); $n = 6$; $^{****}P < 0.0001$ between 0 and 20 μM conditions. (*B*) Levels of LC3B-I and LC3B-II in A549 cells described in *A* treated with 10 μM CQ for 0–16 h. Compared with sgCtrl cells, A549 DKO cells have enhanced LC3B-II accumulation, indicating enhanced autophagic flux. (*C*) Increased accumulation with or without CQ treatment, of endogenous LC3B-II as well as GFP cleavage from exogenously expressed GFP-LC3B in A549 DKO compared with A549 sgCtrl cells. Cells were cultured in the presence of 10% serum with or without 10 μM CQ for 2, 4, or 6 h. In *B* and *C*, β-ACTIN was used as a loading control. (*D*) Fluorescence microscopy images demonstrating increased GFP-LC3 punctae (white arrows) upon loss of *IRS1*/*IRS2* in A549 DKO compared with sgCtrl cells described in *C* that were treated with 10 μM CQ for 6 h. (Scale bars, 25 μM.) (*E*) Quantification of GFP-LC3 punctae in cells from *D*; $n = 15$–20 images per condition; $^*P < 0.05$; $^{**}P < 0.01$. Data are pooled from three independent experiments. (*F*) Proliferation curves of A549 and Calu-1 cells described in *A*, which were grown in 10% serum and treated with MG-132 for 7 d; $n = 6$; $^{****}P < 0.0001$ between 0 and 10 μM conditions for A549 and between 0 and 5 μM as well as 0 and 10 μM for Calu-1. In *A*, *E*, and *F*, data represent the mean ± SD.

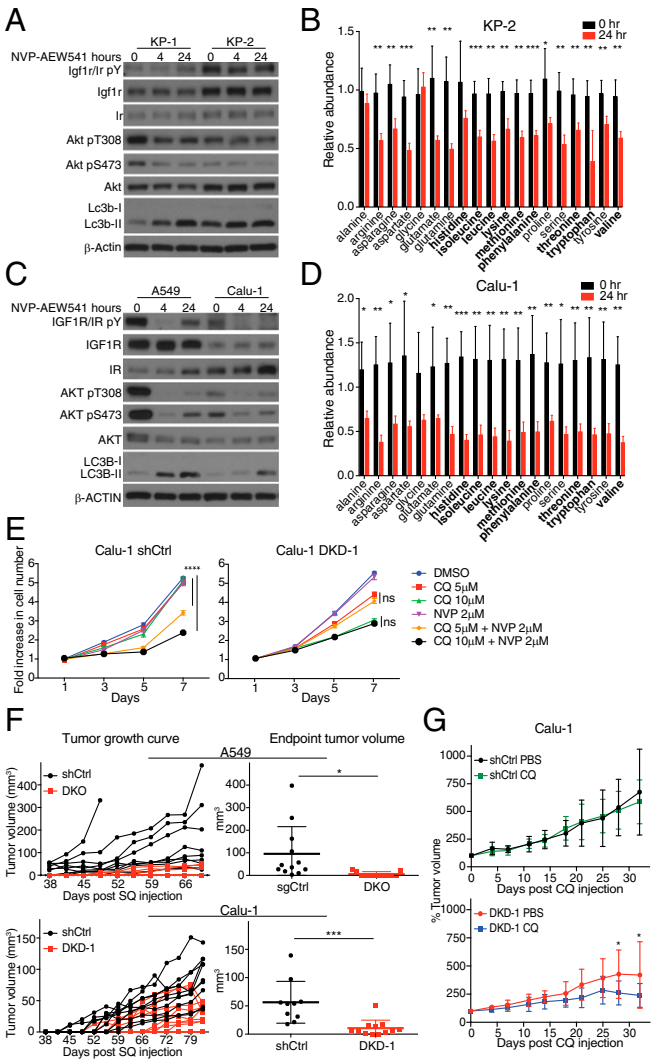

Fig. 5. Acute inhibition of insulin/IGF1 signaling in *KRAS*-mutant lung cancer cells leads to in vivo growth suppression and dependence on autophagy. (*A* and *C*) Levels of total and phosphorylated IGF1R and IR, total and phosphorylated AKT, as well as LC3B-I and LC3B-II in murine *Kras*-mutant, *p53*-null lung cancer (KP) cells (*A*) or NSCLC A549 and Calu-1 cells (*C*) grown in 10% serum and treated with 2 μM NVP-AEW541 for 0, 4, or 24 h; β-ACTIN was used as a loading control. (*B* and *D*) Levels of amino acids in KP cells (*B*) or Calu-1 cells (*D*) cultured in the presence of 10% serum with or without 2 μM NVP-AEW541 for 24 h. Metabolite levels were first normalized to protein levels, and then to the median of all samples for each amino acid; $n = 4$ biological replicates per condition. (*E*) Proliferation curves of Calu-1 shCtrl and DKD cells, which were grown in 10% serum and treated with either vehicle control (DMSO), CQ, NVP-AEW541, or both drugs for 7 d; $n = 4$. Data represent the mean ± SEM. $^{****}P < 0.0001$ between single compound treatment and combinatorial treatment conditions; ns, nonsignificant. (*F*) Growth of individual s.c. xenograft tumors derived from A549 cells (*Top*) over 67 d (one mouse had to be killed at 51 d) and Calu-1 (*Bottom*) over 84 d (*Left*) with endpoint average tumor volume (*Right*); $n = 12$ (A549 sgCtrl); $n = 11$ (A549 DKO); $n = 10$ (Calu-1 shCtrl); $n = 12$ (Calu-1 DKD-1). (*G*) Percent growth of s.c. xenograft Calu-1 tumors with control or *IRS1/IRS2* knockdown in mice treated with vehicle control (PBS) or chloroquine (CQ) (60 mg/kg), 5 d per week for 32 d after median tumor volume reached ~150 mm^3; $n = 8$ (shCtrl PBS); $n = 10$–12 (shCtrl CQ); $n = 10$ (DKD-1 PBS); $n = 10$ (DKD-1 CQ). In *B*, *D*, *F*, *Right*, and *G*, data represent the mean ± SD. $^{*}P < 0.05$; $^{**}P < 0.01$; $^{***}P < 0.001$.

acid availability, generating an increased dependency on protein catabolic pathways to compensate for lower nutrient levels.

To validate the effect of combinatorial inhibition of IR/IGF1R and autophagy, we treated NSCLC cells with either NVP-AEW541, chloroquine, or a combination of both. Although neither drug affected the proliferation of Calu-1 control cells when administered alone at the indicated doses, simultaneous addition of both compounds significantly suppressed their cellular growth (Fig. 5*E*, *Left*). As expected, silencing of *IRS1*/*IRS2* also sensitized Calu-1 DKD cells to chloroquine treatment. Importantly, however, treatment with NVP-AEW541 either alone or in combination with chloroquine did not result in any additional, nonspecific effects upon *IRS1*/*IRS2* knockdown (Fig. 5*E*, *Right*). Similar results were observed in A549 cells (Fig. S4*E*), although the combinatorial treatment of A549 DKD cells using the higher dose (10 μM) but not lower dose (5 μM) of chloroquine resulted in nonspecific toxic effects, indicating that the combinatorial treatment needs to be carefully titrated for different NSCLC cells.

Interestingly, the murine KPI cells, which overcame chronic rather than acute *Irs1*/*Irs2* loss in vivo following prolonged tumor latency (Fig. 1), did not display enhanced autophagic flux nor did they exhibit enhanced sensitivity to CQ treatment (Fig. S6 *A* and *B*). This implies that the KPI cells have adapted alternative mechanisms to overcome the metabolic and growth impairment resulting from chronic loss of *Irs1* and *Irs2*. Indeed, RPPA results revealed that three of four KPI cells had enhanced activation of growth factor receptors other than IR/IGF1R (Fig. S6*C*). In particular, increased phosphorylation of epidermal growth factor (Egfr) on Y1173 and Y1068 was found in both KPI-3 and KPI-5 cells. Moreover, KPI-6 cell line displayed significantly increased phospho-Y1289 Her3. On the other hand, KPI-5 cells exhibited increased levels of platelet-derived growth factor-β (Pdgf-β). Upregulation or activation of these alternative receptor tyrosine kinases may have enabled KPI cells to overcome the loss of *Irs1* and *Irs2* and the resulting suppression of lung tumor growth.

Recently, *Kras*-driven lung cancer was shown to be dependent on BCAA metabolism for nucleotide synthesis and in vivo tumor growth (29). Consistently, we found that loss of *IRS1*/*IRS2*, which results in decreased intracellular levels of essential amino acids, significantly hinders the ability of NSCLC cells to form tumors in vivo. Indeed, whereas all A549 control cells formed xenograft tumors over a period of 10 wk, only 3 of 11 A549 DKO cell injections yielded tumors that, however, grew to a significantly lesser extent than controls (Fig. 5*F*). Similarly, the growth of all Calu-1 xenograft tumors was mitigated upon *IRS1*/*IRS2* knockdown (Fig. 5*F*). Importantly, *IRS1*/*IRS2* silencing sensitized NSCLC preformed tumors to autophagy inhibition, as demonstrated by significantly decreased growth of Calu-1 DKD tumors following chloroquine treatment, compared with vehicle control. In contrast, no significant changes were observed in tumor growth upon chloroquine treatment of mice bearing control knockdown Calu-1 tumors (Fig. 5*G*). Altogether, these results indicate that loss or silencing of *IRS1*/*IRS2* suppresses in vivo growth of *KRAS*-mutant NSCLC and leads to enhanced sensitivity to autophagy inhibition.

To evaluate the respective roles of IR and IGF1R in *KRAS*-driven NSCLC cells, we knocked down each receptor individually in A549 and Calu-1 cells and assessed the knockdown effect on downstream insulin/IGF1 signaling and cellular proliferation. We found that, compared with IR, IGF1R is indeed a dominant receptor in these cancer cells, as its silencing resulted in a more profound suppression of AKT activation (Fig. S7 *A* and *B*). Consistently, whereas *IR* knockdown did not affect the in vitro proliferation of A549 or Calu-1 cells, that of *IGF1R* resulted in significant suppression of cellular growth (Fig. S7 *C* and *D*). These data support the translational relevance and therapeutic potential of using specific IGF1R inhibitors in combination with autophagy/proteasome inhibitors to target NSCLC.

Discussion

Previous work demonstrated that KRAS can bind to and activate PI3K p110α, and that this interaction is required for *KRAS*-driven transformation. Disrupting the Kras–p110α interaction in genetically engineered mouse models of lung cancer suppresses

tumor initiation and causes partial regression of established tumors (6, 7). However, despite its requirement, the sufficiency of KRAS–p110α interaction in driving *KRAS*-driven lung tumor formation, and the need for additional input from growth factor receptors upstream of KRAS and PI3K has remained largely controversial (9). Here, using a conditional genetically engineered mouse model of lung cancer with *Irs1*/*Irs2* loss, we provide robust evidence that insulin/IGF1 signaling is required for *Kras*-driven lung tumor initiation. We show that concomitant expression of *Kras* oncogene and the triple loss of *p53*, *Irs1*, and *Irs2* specifically in lung cells, strongly suppresses *Kras*-driven lung tumor formation. Moreover, we show that *Kras*-transformed lung cells can eventually overcome this suppression, albeit at a stochastic rate and with extended latency.

It is noteworthy that genetic loss of *Irs1* alone in a similar *Kras*-driven mouse model of lung cancer, which however expresses wild-type *p53*, resulted in increased rather than decreased tumor burden and reduced survival (18). This seemingly contradictory result is however not surprising, given that the tumor cells had retained wild-type *Irs2* expression. Although the report did not mention or discuss *Irs2* expression, we find that Irs2 protein levels are significant in both mouse and human *Kras*-mutant lung cancer cells, and that knockdown of *Irs1* either does not affect or rather causes a compensatory increase in the expression of *Irs2*. As a result, Akt activation remains intact in *Irs1* knockdown cells, in response to insulin/IGF1 stimulation (Figs. S2 and S3). Thus, dual genetic ablation of *Irs1* and *Irs2*, but not *Irs1* alone, is required for suppression of Akt activation upon ligand stimulation and suppression of tumor growth.

We find that the late-arising, higher-grade, *Kras*-driven tumors that overcome *Irs1*/*Irs2* loss have decreased E-cadherin levels, a feature of enhanced invasiveness, and a recognized marker of an epithelial-to-mesenchymal transition (EMT) (23). These cells also display significantly decreased intracellular levels of essential amino acids, likely due to decreased amino acid uptake resulting from suppressed growth factor signaling (24–27). Interestingly, in a recent report, EMT was shown to induce autophagy in breast cancer stem cell populations, endowing them with an enhanced ability to escape immune surveillance (30). Thus, a link between EMT, tumor invasiveness, and induction of autophagy deserves further investigation in the *KRAS*-driven NSCLC tumors with suppressed insulin/IGF1 signaling.

Whereas preclinical studies indicated a role for insulin/IGF1 signaling in lung tumor growth, clinical trials showed adverse effects of systemic IGF1R inhibition in unselected patients (8, 31), leaving questionable the relevance of therapeutic targeting of IR/IGF1R in NSCLC patients. Our study highlights the translational relevance of blocking IR/IGF1R signaling specifically in the lungs, leading to strong suppression of tumor formation. Furthermore, it provides a metabolic link between IR/IGF1R signaling and amino acid utilization, as inhibition of such signaling results in decreased intracellular amino acid levels, generating a metabolic dependency of *KRAS*-driven lung tumors on protein catabolic pathways. Consequently, combinatorial targeting of IGF1R and either autophagy or the proteasome may represent a valuable therapeutic strategy in treating *KRAS*-mutant NSCLC.

Materials and Methods

Mouse Studies. Animal studies were approved by the Institutional Animal Care and Use Committee at Boston Children's Hospital. Breeding and adenoviral-Cre infection of KP and KPI mice, xenograft studies, as well as tumor burden quantification and grading are described in detail in *SI Materials and Methods*.

Cell Culture Studies. Tumor dissociation, cell culture, genotyping, imaging of GFP-LC3, immunoblotting and Luminex assay, RPPA protocol, and metabolite quantification are described in detail in *SI Materials and Methods*.

Statistical Analyses. Detailed statistical analyses for both in vitro and in vivo data are described in *SI Materials and Methods*.

ACKNOWLEDGMENTS. We thank the N.Y.K. and M.F.W. laboratory members for thoughtful comments and discussions. This research was supported by Boston Children's Hospital (H.X., M.-S.L., P.-Y.T., A.S.A., N.L.C., S.C., and N.Y.K.) and NIH/National Cancer Institute Grant R01 CA211944 (to N.Y.K.).

1. Siegel RL, Miller KD, Jemal A (2017) Cancer statistics, 2017. *CA Cancer J Clin* 67:7–30.
2. World Health Organization (2017) *Cancer* (WHO, Geneva), Fact Sheet No. 297.
3. Project CG (2017) Catalogue of Somatic Mutations in Cancer (COSMIC) (Wellcome Trust Sanger Institute, Hinxton, UK), Version 80.
4. Imielinski M, et al. (2012) Mapping the hallmarks of lung adenocarcinoma with massively parallel sequencing. *Cell* 150:1107–1120.
5. Stephen AG, Esposito D, Bagni RK, McCormick F (2014) Dragging ras back in the ring. *Cancer Cell* 25:272–281.
6. Castellano E, et al. (2013) Requirement for interaction of PI3-kinase p110α with RAS in lung tumor maintenance. *Cancer Cell* 24:617–630.
7. Gupta S, et al. (2007) Binding of ras to phosphoinositide 3-kinase p110alpha is required for ras-driven tumorigenesis in mice. *Cell* 129:957–968.
8. Pollak M (2012) The insulin and insulin-like growth factor receptor family in neoplasia: An update. *Nat Rev Cancer* 12:159–169.
9. Molina-Arcas M, Hancock DC, Sheridan C, Kumar MS, Downward J (2013) Coordinate direct input of both KRAS and IGF1 receptor to activation of PI3 kinase in KRAS-mutant lung cancer. *Cancer Discov* 3:548–563.
10. White MF, Maron R, Kahn CR (1985) Insulin rapidly stimulates tyrosine phosphorylation of a Mr-185,000 protein in intact cells. *Nature* 318:183–186.
11. Engelman JA, Luo J, Cantley LC (2006) The evolution of phosphatidylinositol 3-kinases as regulators of growth and metabolism. *Nat Rev Genet* 7:606–619.
12. Jackson EL, et al. (2001) Analysis of lung tumor initiation and progression using conditional expression of oncogenic K-ras. *Genes Dev* 15:3243–3248.
13. Jonkers J, et al. (2001) Synergistic tumor suppressor activity of BRCA2 and p53 in a conditional mouse model for breast cancer. *Nat Genet* 29:418–425.
14. Oliver TG, et al. (2010) Chronic cisplatin treatment promotes enhanced damage repair and tumor progression in a mouse model of lung cancer. *Genes Dev* 24:837–852.
15. Dong X, et al. (2006) Irs1 and Irs2 signaling is essential for hepatic glucose homeostasis and systemic growth. *J Clin Invest* 116:101–114.
16. Curry NL, et al. (2013) Pten-null tumors cohabiting the same lung display differential AKT activation and sensitivity to dietary restriction. *Cancer Discov* 3:908–921.
17. Copps KD, Hançer NJ, Qiu W, White MF (2016) Serine 302 phosphorylation of mouse insulin receptor substrate 1 (IRS1) is dispensable for normal insulin signaling and feedback regulation by hepatic S6 kinase. *J Biol Chem* 291:8602–8617.
18. Metz HE, et al. (2016) Insulin receptor substrate-1 deficiency drives a proinflammatory phenotype in KRAS mutant lung adenocarcinoma. *Proc Natl Acad Sci USA* 113:8795–8800.
19. Feldser DM, et al. (2010) Stage-specific sensitivity to p53 restoration during lung cancer progression. *Nature* 468:572–575.
20. Hennessy BT, et al. (2010) A technical assessment of the utility of reverse phase protein arrays for the study of the functional proteome in non-microdissected human breast cancers. *Clin Proteomics* 6:129–151.
21. Saxton RA, Sabatini DM (2017) mTOR signaling in growth, metabolism, and disease. *Cell* 168:960–976.
22. Jeanes A, Gottardi CJ, Yap AS (2008) Cadherins and cancer: How does cadherin dysfunction promote tumor progression? *Oncogene* 27:6920–6929.
23. Brabletz T, Kalluri R, Nieto MA, Weinberg RA (2018) EMT in cancer. *Nat Rev Cancer* 18:128–134.
24. Boerner P, Resnick RJ, Racker E (1985) Stimulation of glycolysis and amino acid uptake in NRK-49F cells by transforming growth factor beta and epidermal growth factor. *Proc Natl Acad Sci USA* 82:1350–1353.
25. Duclos MJ, Chevalier B, Goddard C, Simon J (1993) Regulation of amino acid transport and protein metabolism in myotubes derived from chicken muscle satellite cells by insulin-like growth factor-I. *J Cell Physiol* 157:650–657.
26. Durante W, Liao L, Iftikhar I, Cheng K, Schafer AI (1996) Platelet-derived growth factor regulates vascular smooth muscle cell proliferation by inducing cationic amino acid transporter gene expression. *J Biol Chem* 271:11838–11843.
27. Obata T, et al. (1996) Insulin signaling and its regulation of system A amino acid uptake in cultured rat vascular smooth muscle cells. *Circ Res* 79:1167–1176.
28. Perera RM, Zoncu R (2016) The lysosome as a regulatory hub. *Annu Rev Cell Dev Biol* 32:223–253.
29. Mayers JR, et al. (2016) Tissue of origin dictates branched-chain amino acid metabolism in mutant Kras-driven cancers. *Science* 353:1161–1165.
30. Akalay I, et al. (2013) Epithelial-to-mesenchymal transition and autophagy induction in breast carcinoma promote escape from T-cell-mediated lysis. *Cancer Res* 73:2418–2427.
31. Fidler MJ, Shersher DD, Borgia JA, Bonomi P (2012) Targeting the insulin-like growth factor receptor pathway in lung cancer: Problems and pitfalls. *Ther Adv Med Oncol* 4:51–60.